

See discussions, stats, and author profiles for this publication at: <https://www.researchgate.net/publication/237842366>

A geophysical investigation of the active Hockley Fault System near Houston, Texas

Article in *Geophysics* · July 2013

DOI: 10.1190/GEO2012-0258.1

CITATIONS

18

READS

2,584

4 authors:



Shuhab D Khan

University of Houston

122 PUBLICATIONS 1,702 CITATIONS

SEE PROFILE



Robert R. Stewart

University of Houston

523 PUBLICATIONS 2,786 CITATIONS

SEE PROFILE



Maisam Otoum

United Nations Development Programme

1 PUBLICATION 18 CITATIONS

SEE PROFILE



Li Chang

University of Houston

15 PUBLICATIONS 39 CITATIONS

SEE PROFILE

Some of the authors of this publication are also working on these related projects:



Petroleum Potential of Harris County [View project](#)



Integrative geologic and geophysical studies of active fault zones in Haiti [View project](#)

Case History

A geophysical investigation of the active Hockley Fault System near Houston, Texas

Shuhab D. Khan¹, Robert R. Stewart¹, Maisam Otoum¹, and Li Chang¹

ABSTRACT

Sedimentation and deformation toward the Gulf of Mexico Basin cause faulting in the coastal regions. In particular, many active (but non-seismic) faults underlie the Houston metropolitan area. Using geophysical data, we have examined the Hockley Fault System in northwest Harris County. Airborne LiDAR is an effective tool to identify fault scarps and we have used it to identify several new faults and assemble an updated map for the faults in Houston and surrounding areas. Two different LiDAR data sets (from 2001 to 2008) provide time-lapse images and suggest elevation changes across the Hockley Fault System at the rate of 10.9 mm/yr. This rate is further supported by GPS data from a station located on the downthrown side of the Hockley Fault System indicating movement

at 13.8 mm/yr. To help illuminate the subsurface character of the faults, we undertook geophysical surveys (ground-penetrating radar, seismic reflection, and gravity) across two strands of the Hockley Fault System. Ground-penetrating radar data show discontinuous events to a depth of 10 m at the main fault location. Seismic data, from a vibroseis survey along a 1-km line perpendicular to the fault strike, indicate faulting to at least 300-m depth. The faults have a dip of about 70°. Gravity data show distinct changes across the fault. However, there are two contrasting Bouguer anomalies depending on the location of the transects and their underlying geology. Our geophysical surveys were challenged by urban features (especially traffic and access). However, the survey results consistently locate the fault and hold significant potential to understand its deformational features as well as assist in associated building zoning.

INTRODUCTION

Active faults in the Gulf of Mexico coastal plains were first studied in 1926 as a result of local land-surface subsidence around an oil production field near Galveston Bay (Pratt and Johnson, 1926). Since then, hundreds of active faults have been identified in the Houston metropolitan area (Verbeek et al., 1979; O'Neill and Van Siclen, 1984; Mastroianni, 1991; Shaw and Lanning-Rush, 2005; Engelkemeir and Khan, 2007, 2008). The activity of these faults may have resulted in land-surface subsidence in multiple areas around the coast. Some of the historical subsidence in the greater Houston area has been attributed to the extraction of subsurface hydrocarbons and more recently to groundwater withdrawal (Sheets, 1971, 1979; Paine, 1993; Coplin and Galloway, 1999).

The continuing activity of such widespread down-to-the-coast faults has resulted in an increase in lowland areas near the coast that deform the land surface and have changed drainage pathways. These have given rise to significant interest and concern about fault activity in the Houston metropolitan area.

These faults are mainly identified as growth faults, which are present in most coastal areas including the Houston-Galveston region (Clanton and Amsbury, 1975; Dillon et al., 1982). Historically, these growth faults have played a major role in oil and gas exploration in the Gulf of Mexico. Substantial hydrocarbon accumulations in the Gulf region are often related to growth faults or to salt structures (Ewing, 1983; Shelton, 1984); so, the ability to map faults in such hydrocarbon-promising regions is a key to exploration. Additionally, mapping active faults is essential in areas where potential

Manuscript received by the Editor 8 July 2012; revised manuscript received 12 December 2012; published online 7 June 2013.

¹University of Houston, Department of Earth and Atmospheric Sciences, Houston, Texas, USA. E-mail: sdkhan@uh.edu; rstewar@central.uh.edu; maotoum@mail.uh.edu; li_chang.tw@yahoo.com.tw.

© 2013 Society of Exploration Geophysicists. All rights reserved.

geohazards related to land-surface subsidence prevail. Fault-related subsidence has been recorded in several locations around Houston. Rates vary with location, but some areas have witnessed a subsidence rate of several centimeters per year in northwest Houston (Galloway et al., 1999). In Jersey Village (just outside of Houston) alone, the annual subsidence rate for 30 km² area was recorded at 5.6 cm/yr (Engelkemeir et al., 2010). Fortunately, these deformations have not given rise to substantial seismic events.

In summary, growth faulting, subsidence caused by withdrawal of fluids, and salt tectonics are suggested mechanisms for these faults. The objective of this work is to carry out a detailed integrated study of these faults to identify the key driving mechanisms for faulting in the greater Houston area and its potential societal impact. As a first step toward this goal, this study produces a new map for the surface faults in Houston and surrounding areas using airborne LiDAR data (Figure 1). Second, this work focuses on the Hockley Fault System. This system extends over 12 km in length in northwest Harris county, has a northeast–southwest orientation, and is considered to be the one of the fastest-moving faults in the

region (Figure 1). Although this fault has been known since the early 20th century (Verbeek and Clanton, 1978), very little is known about its subsurface character. The scarp of the main fault has been reported to be about 12 m in height at its northeastern part (Turner et al., 1991; Saribudak, 2011). The main fault scarp crosses a major state highway (Highway 290) that connects Houston with Austin. In addition, a railroad parallel to the highway is also in service. The fault also passes through Fairfield Village, which is a highly populated residential area with over 25,000 residents, and is just next to a large shopping center (Premium Outlet).

Figure 2 shows the general geology and stratigraphy of Harris County. The older Willis Formation (Pleistocene) is primarily composed of clays with lesser amounts of silts and sands (Figure 2a). The Lissie formation (Pleistocene) mainly contains sands with fewer silts and clays, while the Beaumont formation contains finer clays with silt (Moore and Wermund, 1993). The contacts between these formations are zones of low cohesion and thus can become normal faults (Figure 2a). The Hockley Fault System is a good example, because it lies at the contact between the Willis (clay-dominated)

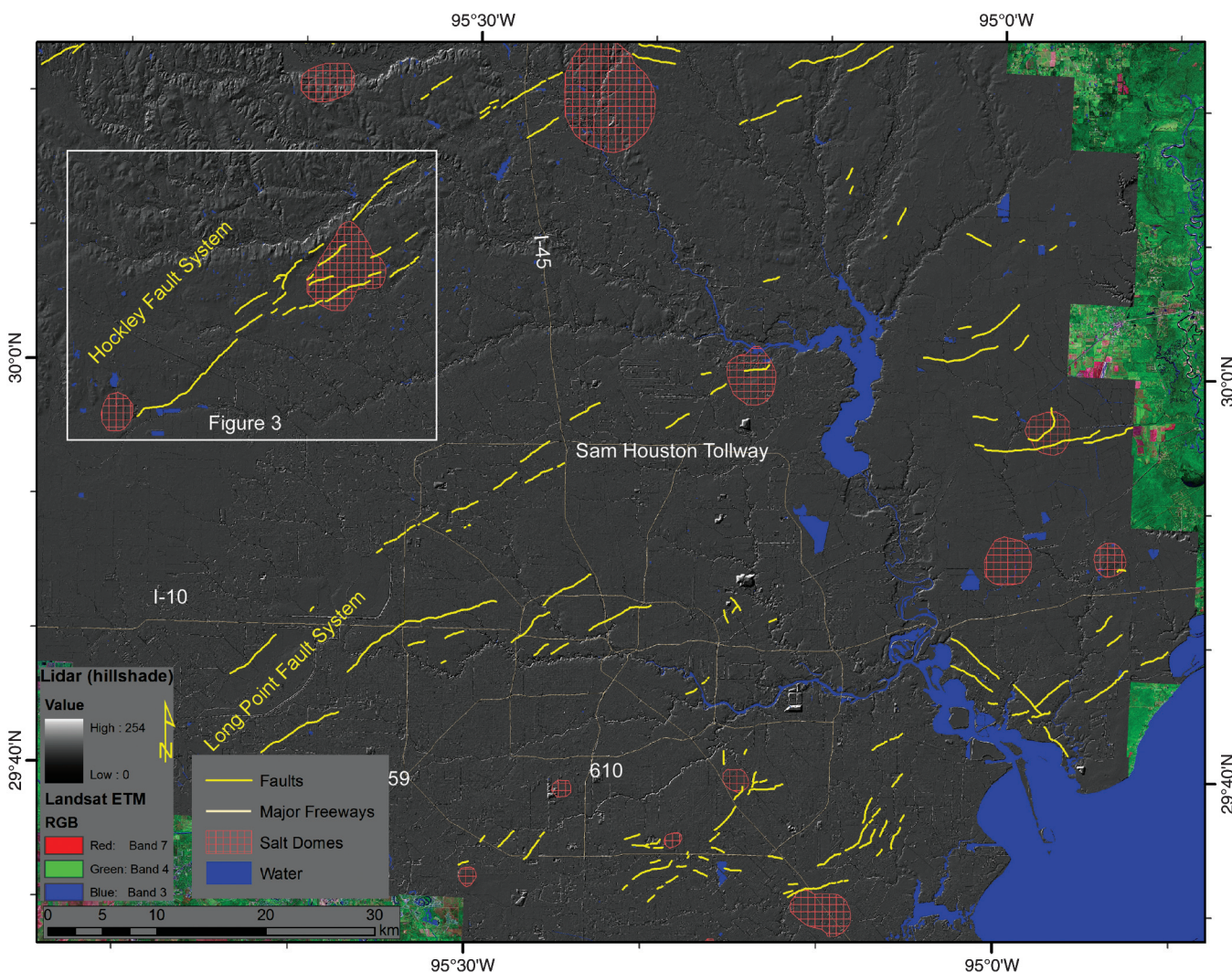


Figure 1. Hillshade image generated from LiDAR DEM data of 2008. These data were used to identify fault scarps in Houston and surrounding areas, as well as salt dome in the subsurface. Salt dome locations are modified from Huffman (2004). Two patterns of faults can be seen; one possibly associated with salt dome and other parallel to the coast line.

and the Lissie (sand-dominated) formations. Fortunately, these deformations have not given rise to substantial seismic events.

DATA AND METHODS

Airborne LiDAR data were used to improve the existing maps of faults in Houston and surrounding areas. Two generations of LiDAR and GPS data were also used to measure the rate of displacement along the Hockley Fault System. In addition, three different geophysical techniques were employed in this study to investigate the Hockley Fault System in the subsurface. Ground-penetrating radar (GPR), seismic reflection, and gravity data were acquired across the fault in two different locations. Figure 3 shows the two locations that were selected based on their exposure to the fault line and accessibility for data acquisition. The first location (location 1 in Figure 3) is at the intersection of the main fault trace and Highway 290. Location 2 is on a private ranch, where a segment of the Hockley Fault System extends about 4 km further to the northeast. The relationship between the two fault segments in the two locations is not clear, but the proximity and the orientation of these two segments suggest that they are part of the larger Hockley Fault System that extends to Tomball, which is approximately 10 km to the northeast from location 2. Both segments are identified on LiDAR images as normal faults dipping to the southeast (Figure 3).

LiDAR

Two sets of airborne LiDAR data are publicly available for the Houston area: 2001, and 2008. The 2001 data set was collected by Terrapoint LLC with horizontal accuracy of ± 0.75 m and vertical accuracy of ± 15 cm. The North American 1983 High Accuracy Reference Network (HARN) (NAD83 HARN) was used as the horizontal datum and the North American Vertical Datum (NAVD) 1988 was used for the vertical datum for both data sets. Merrick & Company collected the 2008 data with horizontal accuracy of ± 0.7 m and vertical accuracy ± 9.25 cm. Each section of LiDAR data had a corresponding digital elevation model (DEM) created. The resolution of the DEM is 3×3 m for the 2001 and 1.5×1.5 m for the 2008 data. Engelkemeir and Khan (2008) used the LiDAR data of 2001 and mapped faults in the Houston area. The 2008 LiDAR data have extended coverage and better resolution; we used DEM and hillshade images generated from 2008 LiDAR data to create an improved map for faults in Houston and its surrounding area (Figure 1).

DEMs can be used to estimate the displacement of surface faults, even faults with minor relief, such as those found in Houston. The height of a fault scarp, measured over years, along a fault trace may provide a measure of fault activity. With DEMs from different time periods, it may be possible to compute the variation in height with time and provide a measure of fault motion for the covered interval. If DEMs are processed differently, direct changes between generations of DEMs can be misleading. These systematic variations can be avoided by adopting procedures that operate on the individual DEMs followed by computation of the scarp height differences. This study uses one such procedure for computing scarp heights from DEMs, which relies upon digitizing pairs of polygons on opposite sides of a fault scarp (Engelkemeir, 2008). The polygons are digitized to provide a consistent estimate of the local elevation and avoid elevation anomalies such as streams and buildings. This estimate is assumed to provide a reasonable measure of the eleva-

tion within the polygon by using the polygons average elevation. A pair of polygons on opposite sides of the fault should then provide a suitable measure of the scarp height across the portion of the fault between the polygons. Several statistical parameters were determined for each polygon for two generation of LiDAR data sets that included elevation attributes of mean, minimum, maximum, and standard deviation. The mean is used for subsequent scarp height computation, whereas the other measurements provide for subsequently evaluating the results of elevation computations. A “throw” is calculated which stores the elevation difference for each polygon pair. Thirty-six pairs of polygons were used on the up and down-thrown sides of the Hockley Fault System. Finally, the differences between the two sets of throws for two generations of DEM were computed, giving way to the slip rate.

Faults are often characterized as a surface of dislocation between earth materials on opposite sides, although a zone of shearing better characterizes many faults. The displacement can be decomposed into throw and heave components, where throw measures the vertical displacement and heave the horizontal. Normal faults generally are steeply dipping ($>60^\circ$), in the near surface, so the throw component is often larger. Also indicative of normal faulting is an increase in slip from their tips towards the middle of the fault (Densmore et al., 2005). The amount of slip also provides an

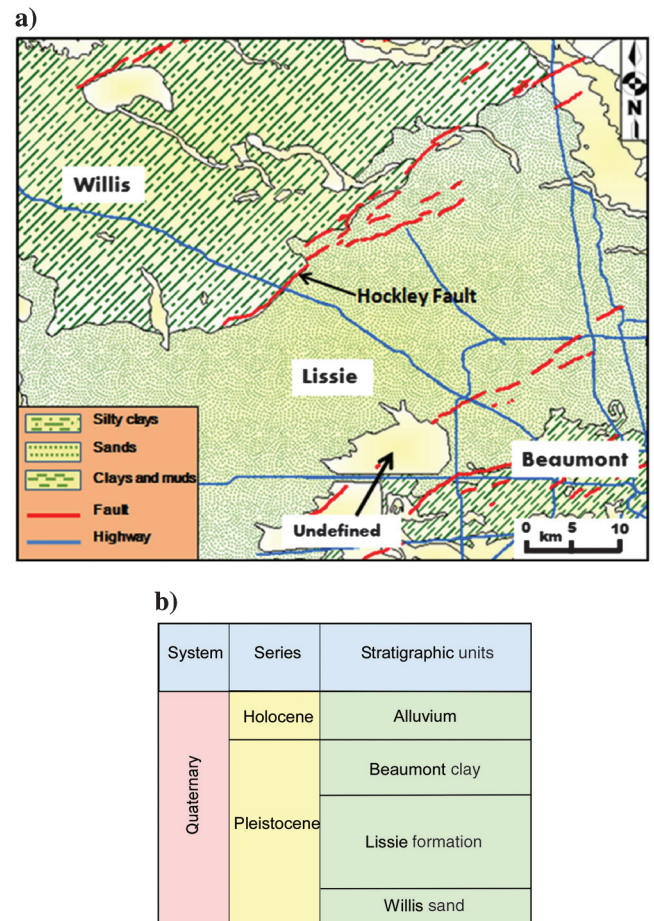


Figure 2. (a) A geologic map of Harris County showing the three major formations: the Willis, the Lissie, and the Beaumont (modified from Bureau of Economic Geology, 1992). (b) Stratigraphic column for Quaternary formations in Harris County.

indication of the amount of recent local activity along different portions of a fault (Roberts and Michetti, 2004). Erosion also modifies the shape of fault scarps and makes determination of heave more difficult than throw. The polygon technique was employed to examine the rate of displacement along the Hockley Fault System (Figure 4a). The average elevation within a polygon is assumed to provide a reasonable measure of the elevation within the polygon. A pair of polygons on opposite sides of the fault should then provide a suitable measure of the scarp height across the portion of the fault between the polygons.

GPS

To check results on the rate of movement along the Hockley Fault System obtained from LiDAR data, GPS data have been processed. The Harris-Galveston Subsidence District (HGSD) in partnership with National Geodetic Survey (NGS) employs a network of GPS stations called periodically active monitors (Middleton, personal

communication, 2011) in conjunction with continuously operating reference station (CORS) to monitor subsidence (Zilkoski et al., 2003). Most of the GPS sites are intentionally kept away from salt domes and active faults; fortunately, one GPS site, PAM 48 (Figure 3), is located not far from the Hockley Fault System on its downthrown side. We obtained raw data for this site from HGSD starting from April 2007 to September 2011. Raw data were converted to Receiver Independent Exchange (RINEX) format and were submitted to Online Positioning User Service (OPUS). OPUS is an online, differential GPS postprocessing application developed by the National Geodetic Survey that provides very reliable and accurate data.

GPR

GPR data were acquired along 2D profiles using the GSSI SIR-3000 system with two sets of antennae: a 400 MHz antenna mounted on a cart system, which provided images to approximately four meters depth and a 100 MHz antenna system that provides up to ten

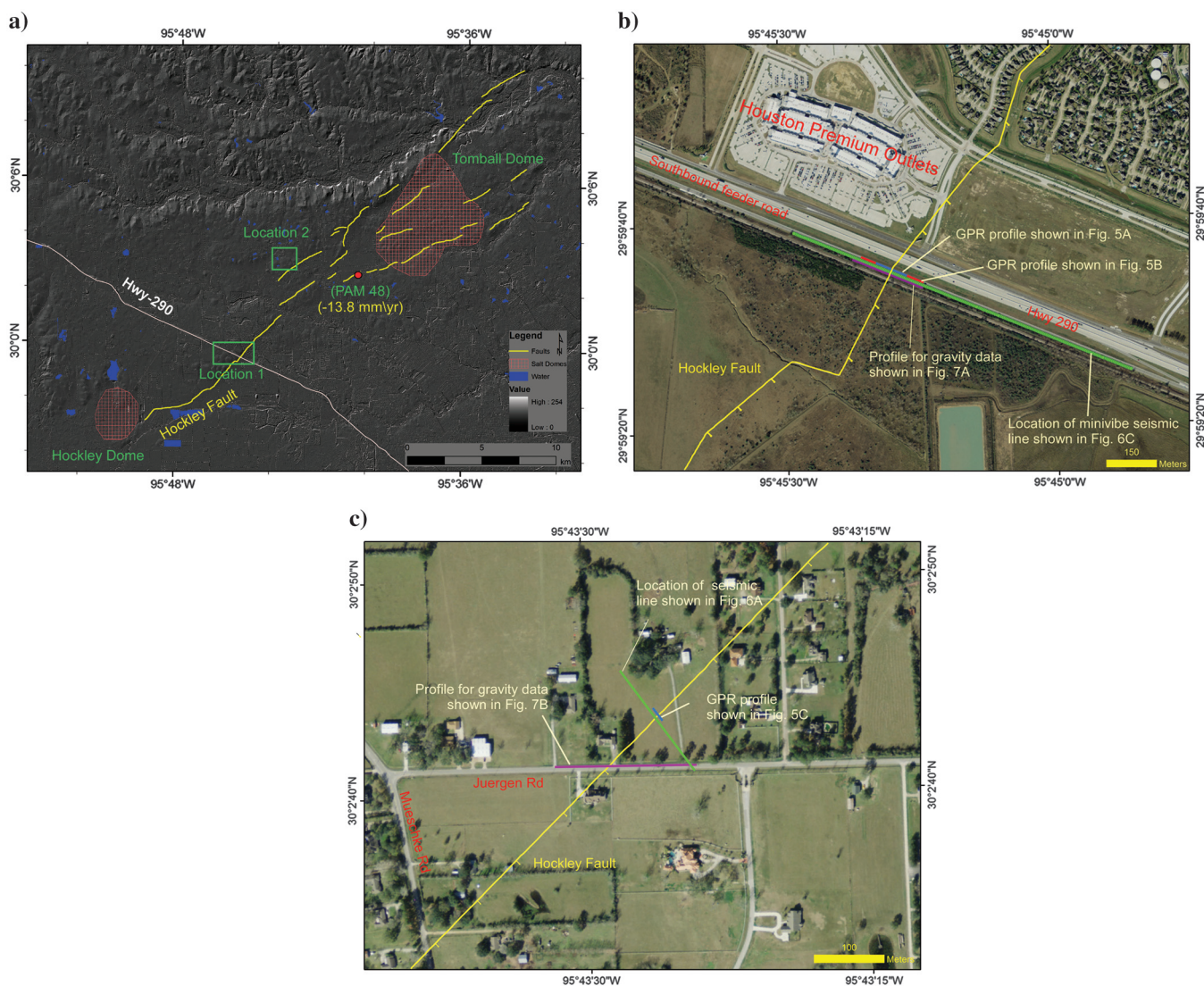


Figure 3. (a) LiDAR hillshade image showing detailed map of the Hockley Fault System. Notice that the Hockley Fault System is bounded by Hockley and Tomball salt domes at the two ends. (b) Map showing locations of GPR, minivibe seismic, and gravity profiles along the feeder road of highway 290. (c) Map of location 2 showing sites of GPR, seismic, and gravity surveys.

meters of imaging. Several GPR profiles are acquired across the Hockley Fault System at both locations.

Acquisition parameters include a gain function that helps counteract the natural earth attenuation of the signal, as well as a band-pass filter to maintain frequencies within the signal band. Postsurvey processing is carried out using RADAN 6.6 software. A conventional processing flow is used for data processing: The positional correction tool removes the air wave. A range-gain balances the amplitudes and final band-pass filters are subsequently applied (50–500 MHz for the 400 MHz antenna and 25–125 MHz for the 100 MHz data). A dielectric constant of 13 is used for both data sets for depth corrections. Deconvolution is also applied to sharpen the pulse signature and highlight finer details. In addition, spatial filters are used to suppress laterally discontinuous traces. The processed GPR profiles are shown in Figure 5 and described further in the results and interpretation section.

Seismic surveys

Two test seismic lines were acquired across the Hockley Fault System in locations 1 and 2 (Figure 3) using a 10-lb hammer source. The seismic line in location 1 has a very low signal-to-noise ratio due to its proximity to the busy Highway 290 and relatively weak source. We note that vehicles moving at 120 km/hr have wheels that are rotating at about 10 cycles per second or 10 Hz — which is in the range of the dominant seismic noise. Because of these noise problems, we collected another test line at location 2 on a quiet ranch site, away from busy roads that resulted in better data quality. This second seismic line has a total length of 177 m and uses 60 vertical-component geophones spaced at 3 m. The hammer source impacts at 3-m intervals between receivers giving a nominal fold of thirty. The record length and the time sampling interval are set to 2 s and 0.25 ms, respectively. Both values were later modified in processing. The line is oriented so that it crosses the fault at about 90° with the surface trace of the fault in the middle zone of the survey line. A stacked section was created after velocity analysis of the common midpoint (CMP) gather. Stacking velocities range from about 1000 m/s in the near surface to 2000 m/s at depth (500 ms two-way traveltime). Noise reduction, including f - x deconvolution, is applied to the data. Poststack and then prestack time migrations are undertaken (the prestack migration is shown in Figure 6a). In March 2012, we returned to the fault area where it crosses Highway 290, with a larger source — the IVI T15000 Minivib. We undertook a 1075 m 2D line with a fixed spread of 216 vertical geophones spaced at 5 m. The vibrating points are every 5 m on the ½ station with a three-fold vertical stack. We used a 12-s sweep from 8 to 150 Hz with a 1-ms sample interval and 16-s listen time, which resulted in a 4-s correlated record. Processing steps include

band-pass filtering, shot deconvolution, f - k filter, velocity analysis, CMP stack, and prestack time migration. The stacking velocity section and a prestack time migration are shown in Figure 6b and 6c.

Gravity

Gravity data were acquired along two profiles collocated with the seismic data. Results show significant variations in the gravity readings on either sides of the fault. Locations 1 and 2 (Figure 3) have contrasting gravity results that have been related to the different geologic formations present in the two areas. In general, gravity data show consistency in describing the fault, especially when linked to the regional geology of the Hockley Fault System area.

The first gravity profile at location 1 is a 225-m line along the southbound feeder road of highway 290 (parallel to GPR profiles 1 and 4, with the fault line at the 122-m marker). The station interval for this profile was 5 m (Figure 7a). The second profile (location 2)

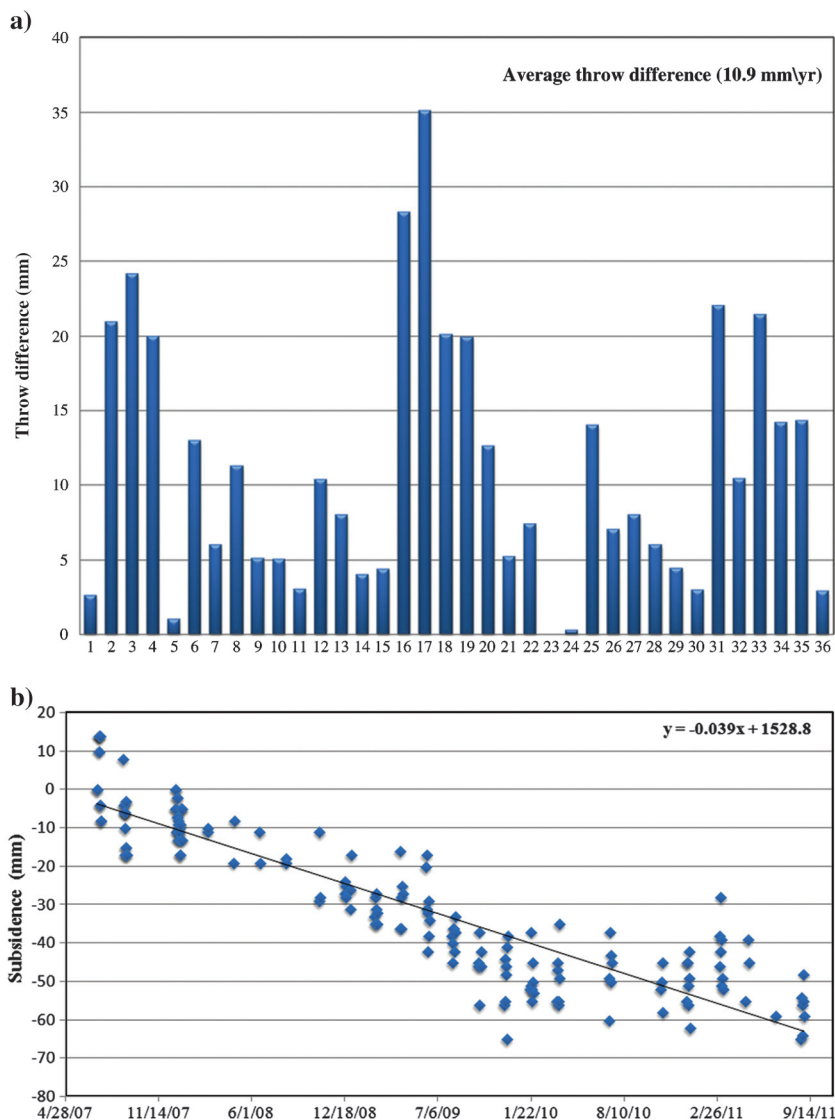


Figure 4. (a) Throw difference for the Hockley Fault System. Throws are computed using pairs of polygons on two sides of the entire length of the fault. (b) Processed GPS data for PAM site 48 in northwest Harris County from 4/2007–9/2011. This site is located on the downthrown side of the Hockley Fault System.

is a 200-m profile with 10-m station interval (Figure 7b). The gravity data were acquired using a Scintrex CG-5 Autograv system with 0.01 mGal accuracy.

Data have been processed using the conventional gravity correction formulas. These formulas include latitude, free-air, and Bouguer corrections. Drift correction is done in the gravity system during acquisition. Temporal corrections are unnecessary because the acquisition took place in short periods of time. A terrain correction is not used because of the relatively constant elevation around the fault. Because of this short line, the latitude correction gives little change.

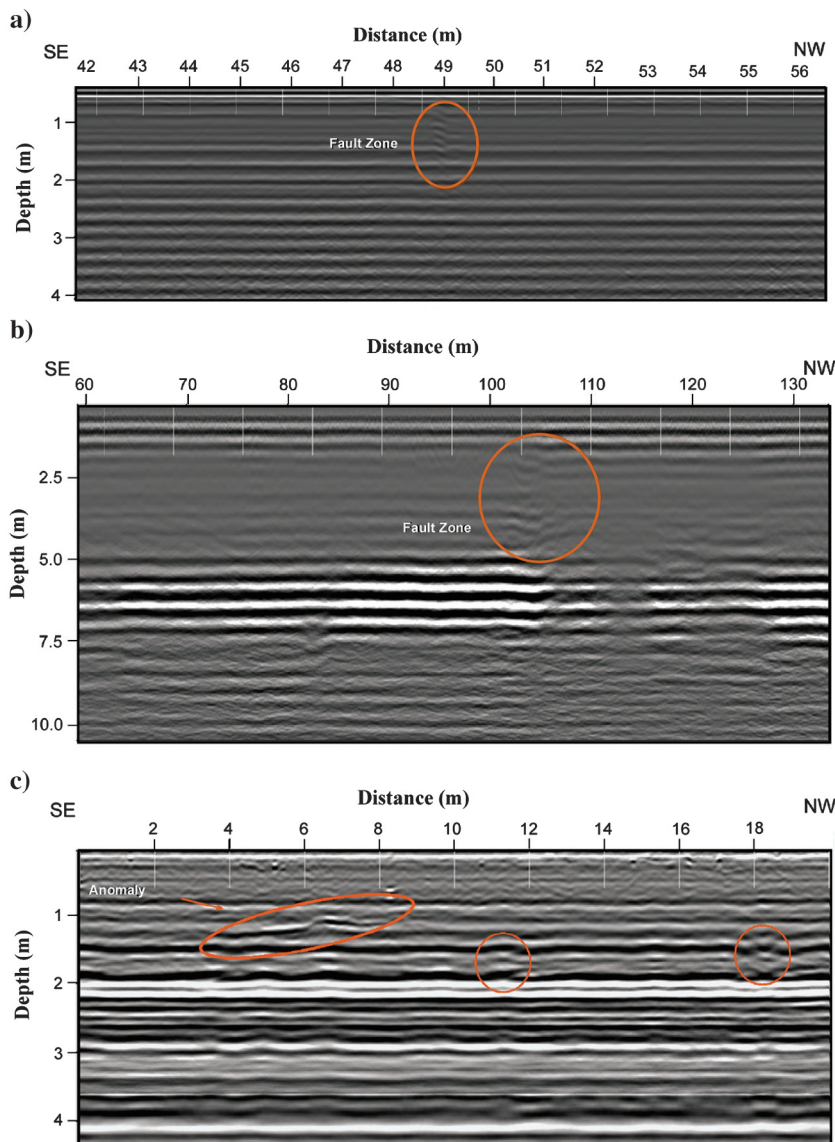


Figure 5. (a) GPR profile acquired at location 1 using 400-MHz antenna. A major discontinuity is observed at the location where the fault is exposed at the surface (at about 49 m). (b) GPR profile acquired at location 1 using a 100-MHz antenna. An image down to 10-m depth is obtained in which two main features outline the fault zone. The loss of amplitude between the two events may be attributed to potentially loose sediments next to the faulted layers. (c) GPR survey line moving up dip perpendicular to the fault scarp at location 2 using 400-MHz antenna. Several anomalies are identified close to the surface exposure of fault.

RESULTS AND INTERPRETATION

LiDAR and GPS

Using the LiDAR data acquired in 2008, we mapped the surface faults in Houston and its surrounding areas. We used the locations of published faults (Verbeek, 1979; Shah and Lanning-Rush, 2005; Engelkemeir and Khan, 2008) and employed hillshade images as a guide for fault interpretation. Our new map, shown in Figure 1, is more exact than earlier versions because scarp locations are mapped with an accuracy of less than one meter. We have identified several new faults or segments of faults (Figure 1) and extended the fault map to the immediate surroundings of Harris County. We have also modified the locations of several salt domes (Huffman, 2004). Many faults are associated with salt domes and show a radial pattern. However, the general trend of most of these faults is northeast–southwest, an orientation that parallels the Gulf of Mexico coast line. Furthermore, most of these faults pass through major highways, residential, and business areas, creating potential risks. Long-term movement along these faults can lead to slow-paced structural damage. The Hockley Fault System is one of these and we have mapped several new segments of it (Figure 3).

Thirty-six pairs of polygons were drawn on the upthrown and downthrown sides of the Hockley Fault System starting at the Hockley Dome and ending at the Tomball Dome. Average elevation values within each polygon for a specified DEM were then computed. The scarp height between pairs was also computed. This resulted in two polygon sets corresponding to the two different generations of LiDAR DEMs (2001, 2008), which were then used to calculate the throw of the fault for each polygon pair. The differences between the two sets of throws gives the slip rate. These throw differences are plotted in Figure 4a; the differences are variable across the length of fault ranging from no dip movement to the maximum of 35 mm/yr of displacement. Generally, the difference is more near the center of the fault and shows an average slip rate of 10.9 mm/yr.

Data acquisition at this site, which started in April 2007, is the only GPS site closest the fault. To check the validity of slip rates, GPS data for the PAM 48 station were processed. The site is located on the downthrown fault side. More than four years of data give an average rate of -13.8 mm/yr of vertical displacement (Figure 4b).

GPR

Figure 5a and 5b shows GPR profiles acquired in location 1 (Figure 3). Figure 5a shows a portion of the 100-m line acquired using a monostatic 400-MHz antenna in June of 2011. A discontinuous event can be seen at the 49-m marker down to a depth of 4 m. Migration for

of this data set does not provide a better image and is dropped from the processing flow. The 400-MHz antenna provides signal penetration up to 4 m; but a more conclusive fault investigation requires deeper imaging. Thus, we used another lower-frequency antenna system (100 MHz). This bistatic antenna system is operated using an antenna separation of 1.5 m. A 200-m-long profile was acquired on the southbound feeder road of Highway 290 with the fault line at position 100 m (Figure 3b). The 100 MHz system provided reasonable data quality up to about 10-m depth. Figure 5b shows the 100-MHz profile displaying several events seen around the fault. The main fault zone is identified by two major discontinuous events around the center of the profile (105–120 m in Figure 5b). The high signal attenuation within the fault zone may be caused by loose sediments with high water content, created by the fault activity. The dip angle of the event at 105 m is approximately 70° .

We also conducted a 2D GPR survey at location 2, using the 400-MHz antenna. A 20-m-long profile was acquired perpendicular to the fault. Figure 5c shows the processed GPR line. Several anomalies were detected across this line. The large anomaly around 6 m in Figure 5c suggests a reflector bending up dip in response to faulting. Around 11.5 m and 18 m, smaller anomalies are detected showing discontinuities in the reflections. The strong linear amplitudes at about a 2-m depth may represent the water table.

Seismic data

The processed hammer seismic data, at location 2, indicates stacking velocity changes along the line. We found a general lowering of velocity from northwest to southeast across the fault. This seems to be consistent with younger, less consolidated materials on the downthrown side of the fault. The migrated section (Figure 6a) is somewhat “wormy,” but we might imagine that the central part of the section is disturbed and may correspond to a faulted region.

The hammer seismic results are not deeply compelling, so as mentioned previously, we returned to the area with a larger vibrator source. The field records from the IVI Minivibe are heavily contaminated with road noise from the Highway 290. However, after low-cut (30-Hz) filtering and further processing, the data have remarkably improved. The final migrated section (Figure 6c) gives a fascinating image, which we interpret to show several possible faults. The surface expression of one fault (a crack on the highway) is near 400 m. We note that there is an anticlinal anomaly at about 100 ms below the surface faults at both line locations. We estimate the dip of the faults as about 70° (using an average velocity of 1500m/s). Surprisingly, there is also some evidence of northwest dipping faults around this same location. A deeper structure, perhaps asso-

ciated with the nearby Hockley salt dome, can be interpreted in the section.

Gravity

Gravity data acquired at location 1 (Figure 3) are shown in Figure 7a. A gravity anomaly (on top of the fault) is 0.3 mGal. This

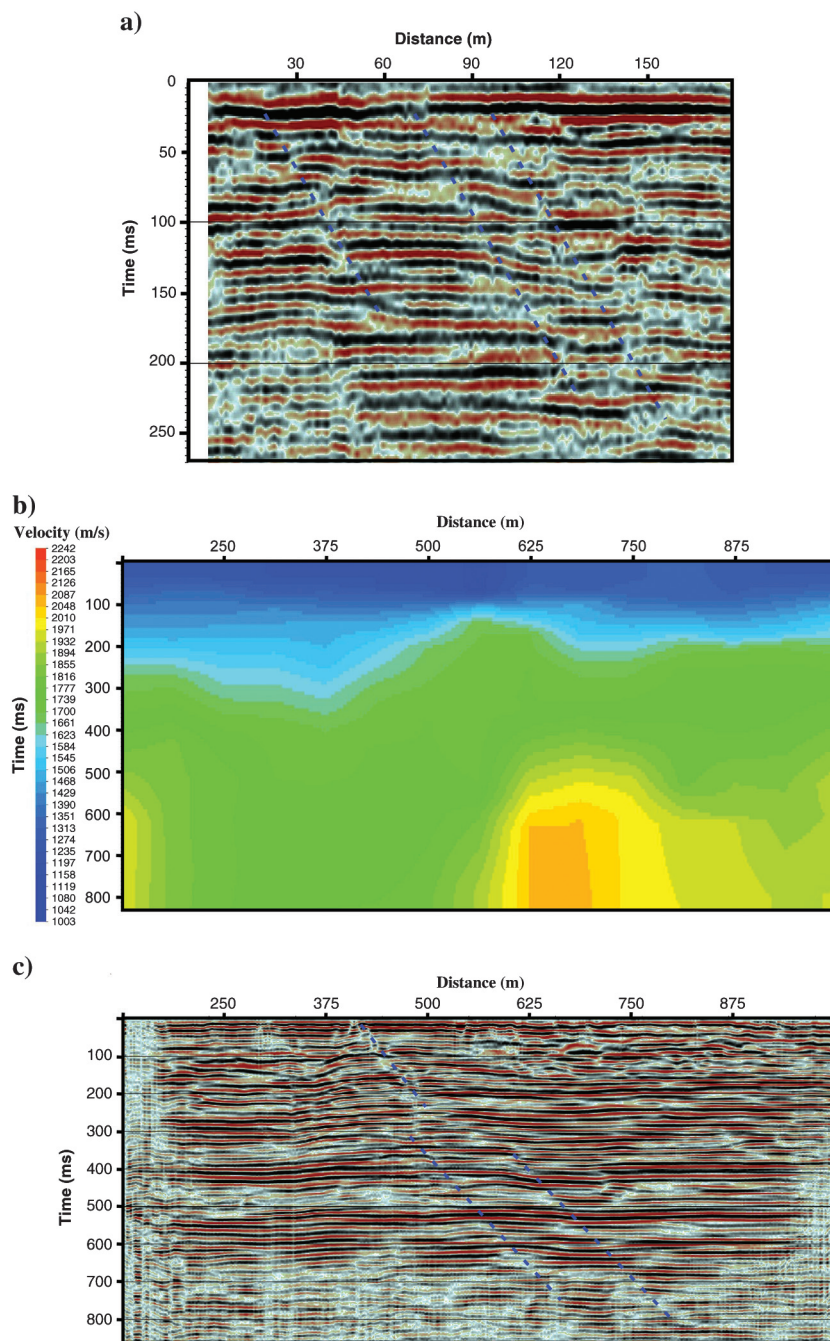


Figure 6. (a) A 180-m-long hammer-seismic test line (migrated section) crossing the Hockley fault system. The fault surface expression is at location 90 m. Possible faults are annotated. (b) Stacking velocities estimated from velocity analysis of the minivibe test line located on Highway 290. (c) Migrated seismic section of a 1000-m minivibe line (CDPs 1 through 401). CDP stations are spaced every 2.5 m. Possible faults are annotated. The fault surface location is at about 400 m.

DISCUSSION

anomaly is in contrast to the conventional gravity signature of faults. Usually, higher gravity is observed on the upthrown side of the fault, and low gravity on the downthrown side, but this profile indicates the opposite. This may be explained by the geologic variation around the Hockley Fault System. The fault lies at the boundary of two different formations; the clay-dominated Willis formation on the upthrown side, and the sand-dominated Lissie formation on the downthrown side. The sand has a higher density than the clays, which might give rise to the increased gravity response on the downthrown side (Athy, 1930). It is also conceivable that salt may be a factor. For the profile in location 2 (shown in Figure 7b), the gravity anomaly shows high values on the upthrown side (with a total difference of 0.15 mGal). The 200-m profile lies entirely within the Lissie formation; thus, we suggest that younger and less dense materials are on the downthrown side and give a gravity decrease.

In summary, gravity data show anomalies at the fault location. The low gravity data response difference suggests that the Lissie formation is thin at this location (a few meters thick), which is consistent with the deposition pattern of sediments near the Gulf coast where formations grow thicker towards the coast.

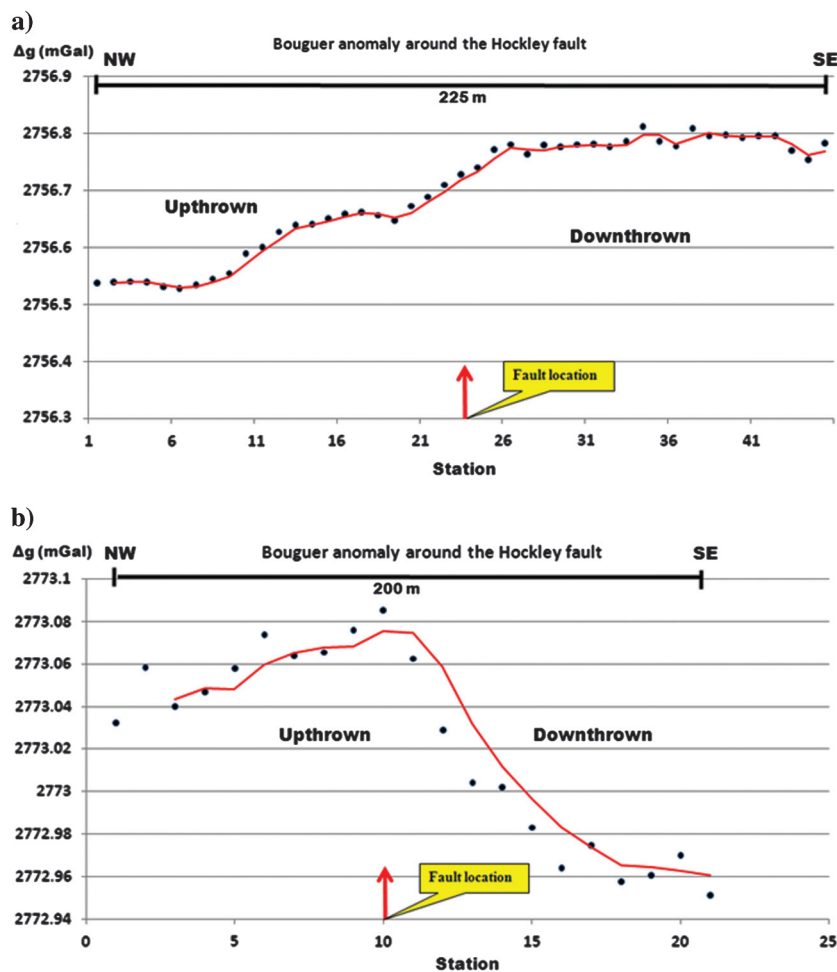


Figure 7. (a) Bouguer anomaly around the Hockley Fault System in location 1. Higher gravity readings are observed on the downthrown side. (b) Bouguer anomaly around the Hockley Fault System in location 2. Higher gravity readings are observed on the upthrown side.

Airborne LiDAR is a powerful tool for mapping surface faults with meter accuracy. The bare-earth DEM, generated from LiDAR and other derivative products like hillshading, proved helpful in the identification of several new faults and new segments of known faults in the Houston area. We found that multiple generations of LiDAR data in conjunction with GPS data can provide decent estimates of displacement along faults. Two sets of DEM models derived from LiDAR data acquired in 2001 and 2008 indicate elevation changes at the Hockley Fault System. They give slip rates of around 10 mm/yr. GPS data shown in Figure 4b show significant decrease in subsidence starting in 2010. Harris-Galveston Subsidence District reports that the northwest of Harris County, where the Hockley Fault System is located, showed a significant drop in groundwater withdrawal in 2010; it changed from the total groundwater withdrawal of 280 million gallons per day in 2000 to 195.5 million gallons per day in 2010 (Lackey, 2011).

Data from the three geophysical techniques used to image the Hockley Fault System all show anomalies at the surface fault location. Two-dimensional GPR profiles collected at two locations on

Hockley Fault System show several discontinuities in the GPR sections that not only detected the main fault, but also present some extra detail regarding the disturbed faulted zone. The dip angle of the main fault is estimated at about 70° based on the GPR data results.

The hammer-seismic signal in the 180-m seismic line at location 2 (Figure 3a) is not strong enough to provide a deep image of the fault. But, the final section indicates some discontinuities underneath the fault line. The minivibe data provided a much better picture of the subsurface to depths of about 600 m, which delivered evidence that the main fault area extends to at least 300 m with a dip of about 70°. In addition, there is a deeper feature that might be related to the nearby Hockley Salt Dome.

The gravity data presents useful information about differing subsurface densities across the fault. The gravity variation across the fault in both profiles is modest — about 0.1–0.3 mGal, whereas the gravity curve in Figure 7a is interesting in that it differs from the conventional case. We suggest that the more dense and sandy Lissie formation appearing on the downthrown side versus the clayey Willis formation give rise to this anomaly. The results from gravity profile 2 (Figure 7b) match the conventional case because the upthrown and the downthrown sides of the fault lie within the Lissie formation.

CONCLUSION

Time-lapse airborne LiDAR has provided a broad areal image of the fault structure and their changes near Houston, Texas. The Hockley Fault System has been investigated in further detail with a variety of contact geophysical methods. These various types of measurements can

complement each other in terms of depth of penetration, resolution, and areal coverage. GPR data proved useful for identifying the fault zone down to about a 10-m depth. Seismic data showed discontinuities and velocity variations around the fault to depths of several hundred meters. Gravity data suggested a fault signature on two curves correlated with the lithological variations in the subsurface. The geophysical methods used in this study indicated a rapidly displacing fault system with dips around 70°, which extend some hundreds of meters into the subsurface.

ACKNOWLEDGMENTS

We express our appreciation to the Allied Geophysical Lab at the University of Houston for its assistance with the seismic especially. Xu Han, Zheng Huang, Kaitlin DeBoer, Kiristi Haynie, and other students from GeoRS Lab of the University of Houston are thanked for their contribution in data acquisition and processing. We are also thankful to GEDCO, Calgary for their donation of the VISTA seismic processing package to us.

REFERENCES

- Athy, L. F., 1930, Density, porosity, and compaction of sedimentary rocks: AAPG Bulletin, **14**.
- Bureau of Economic Geology, 1992, Geologic Map of Texas: University of Texas at Austin, Virgil E. Barnes, project supervisor, Hartmann, B. M., and D. F. Scranton, cartography, scale 1:500,000.
- Clanton, U. S., and D. L. Amrsbury, 1975, Active faults in southeastern Harris County, Texas: Environmental Geology, **1**, 149–154, doi: [10.1007/BF02428942](https://doi.org/10.1007/BF02428942).
- Coplin, L. S., and D. L. Galloway, 1999, Houston-Galveston, Texas: Managing coastal subsidence, in D. L. Galloway, D. R. Jones, and S. E. Ingebritsen, eds., Land subsidence in the United States: U. S. Geological Survey Circular 1182, 35–48.
- Densmore, A. D., N. Gupta, and S. Guidon, 2005, What sets topographic relief in extensional footwalls?: Geology, **33**, 453–456, doi: [10.1130/G21440.1](https://doi.org/10.1130/G21440.1).
- Dillon, W. P., P. Popenoe, J. A. Grow, K. D. Klitgord, B. A. Swift, C. K. Paull, and K. V. Cashman, 1982, Growth faulting and salt diapirism: Their relationship and control in the Carolina Trough, Eastern North America, in J. S. Watkins, and C. L. Drake, eds., Studies of Continental Margin geology: AAPG Bulletin, **34**, 21–46.
- Engelkemeir, R., 2008, Evaluating Houston Area Neotectonics Using GIS and Remote Sensing Techniques: Ph.D. Dissertation, University of Houston.
- Engelkemeir, R., and S. D. Khan, 2007, Near-surface geophysical studies of Houston faults: The Leading Edge, **26**, 1004–1008, doi: [10.1190/1.2769557](https://doi.org/10.1190/1.2769557).
- Engelkemeir, R., and S. D. Khan, 2008, LiDAR mapping of faults in Houston, Texas, USA: Geosphere, **4**, 170–182, doi: [10.1130/GES00096.1](https://doi.org/10.1130/GES00096.1).
- Engelkemeir, R., S. D. Khan, and K. Burke, 2010, Surface deformation in Houston, Texas using GPS: Tectonophysics, **490**, nos. 1–2, 47–54, doi: [10.1016/j.tecto.2010.04.016](https://doi.org/10.1016/j.tecto.2010.04.016).
- Ewing, T. E., 1983, Growth faults and salt tectonics in the Houston diapir province: Relative timing and exploration significance: Transactions of the 33rd Annual Meeting of the Gulf Coast Association of Geological Societies, 83–90.
- Galloway, D. L., D. R. Jones, and S. E. Ingebritsen, eds., 1999, Land subsidence in the United States: U. S. Geological Survey Circular 1182, 177.
- Huffman, A. C., 2004, Salt diapirs in the Gulf Coast. U. S. Geological Survey, DS-90, version 1.0.
- Lackey, M. G., 2011, Annual groundwater report: 33rd Annual Report, s.l., Harris-Galveston Subsidence District, 147.
- Mastroianni, J. J., 1991, A study of active fault movement, Houston, Texas and vicinity, M.S. thesis: University of Houston, 140.
- Moore, D. W., and E. G. Wermund Jr., 1993, Quaternary geologic map of the Austin 4 × 6 degree quadrangle, United States: U. S. Geological Survey Miscellaneous Investigations Series Map I-1420 (NH-14), scale 1:1,000,000.
- O'Neill, M. W., and D. C. Van Siclen, 1984, Activation of Gulf Coast faults by depressuring of aquifers and an engineering approach to siting structures along their traces: Bulletin - Association of Engineering Geologists, **21**, 73–87.
- Paine, J., 1993, Subsidence of the Texas coast: Inferences from historical and late Pleistocene sea levels: Tectonophysics, **222**, 445–458, doi: [10.1016/0040-1951\(93\)90363-O](https://doi.org/10.1016/0040-1951(93)90363-O).
- Pratt, W. E., and D. W. Johnson, 1926, Local subsidence of the Goose Creek oil field, Journal of Geology, **34**, 577–590, doi: [10.1086/623352](https://doi.org/10.1086/623352).
- Roberts, G., and A. Michetti, 2004, Spatial and temporal variations in growth rates along active normal fault systems: An example from the Lazio-Abruzzo Apennines, central Italy: Journal of Structural Geology, **26**, 339–376, doi: [10.1016/S0191-8141\(03\)00103-2](https://doi.org/10.1016/S0191-8141(03)00103-2).
- Saribudak, M., 2011, Geophysical mapping of the Hockley growth fault in northwest Houston, USA, and recent surface observations: The Leading Edge, **30**, 172–180, doi: [10.1190/1.3555328](https://doi.org/10.1190/1.3555328).
- Shaw, S., and J. Lanning-Rush, 2005, Principal faults in the Houston, Texas, metropolitan area: U. S. Geological Survey Scientific Investigations Map 2874.
- Sheets, M. M., 1971, Active surface faulting in the Houston area, Texas: Houston Geological Society Bulletin, **13**, 24–33.
- Sheets, M. M., 1979, Oil fields, subsidence and surface faulting in the Houston area: Houston Geological Society Guidebook, 24.
- Shelton, J., 1984, Listric normal faults: An illustrated summary: AAPG Bulletin, **68**, 801–815.
- Turner, Collie and Braden, Inc., 1991, Feasibility study for the implementation of a water reuse project in Fairfield village: Final internal report, Job No. 22-00080-020.
- Verbeek, E. R., 1979, Surface faults in the Gulf coastal plain between Victoria and Beaumont, Texas: Tectonophysics, **52**, 373–375, doi: [10.1016/0040-1951\(79\)90248-8](https://doi.org/10.1016/0040-1951(79)90248-8).
- Verbeek, E. R., and U. S. Clanton, 1978, Map showing faults in the southeastern Houston metropolitan area, Texas: U. S. Geological Survey Open File Report 78–79.
- Zilkoski, D., L. Hall, G. Mitchell, V. Kammula, A. Singh, W. Chrismer, and R. Neighbors, 2003, The Harris-Galveston Coastal Subsidence District/ National Geodetic Survey Automated GPS Subsidence Monitoring Project: Proceedings of the U. S. Geological Survey Subsidence Interest Group Conference, OFR, 303–308.